J Electroceram (2012) 28:172–177
DOI 10.1007/s10832-012-9702-y

Low-temperature dielectric properties of double-perovskite Ca_2CoNbO_6

G. J. Wang · C. C. Wang · S. G. Huang · X. H. Sun · C. M. Lei · T. Li · J. Y. Mei

Received: 8 December 2011 / Accepted: 27 February 2012 / Published online: 14 March 2012

Abstract Double-perovskite Ca_2CoNbO_6 (CCNO) ceramics were prepared via the solid-state reaction route. Their dielectric properties were investigated as a function of temperature (between 100 and 330 K) in the frequency range from 40 Hz to 10 MHz. Two thermally activated dielectric relaxations were observed with the activation energy around 0.13 eV for the low-temperature relaxation and 0.37 eV for the high-temperature relaxation. Annealing in O_2 and N_2 can remarkably change the dielectric constant, background, relaxation peak intensity and position, etc. These results can be well explained based on the fact that both oxygen and cobalt vacancies coexist in the sample. The low-temperature relaxation was found to be related to the dipolar effect due to the hopping holes, and the high-temperature relaxation was associated with the defect relaxation caused by oxygen and cobalt vacancies.

Keywords Double-perovskite · Dielectric properties · Relaxation · Impedance analysis

1 Introduction

Double-perovskite oxides with general formula $A_2BB'O_6$ have been attracting much attention in recent years because of their peculiar magnetic and electronic properties due to different cations occupying the octahedral site of the primitive perovskite unit cell. This circumstance permits the strong interaction between electronic, magnetic, and structural degrees of freedom that creates a great variety of physical and chemical properties [1]. For example, the complex perovskite system can easily create properties such as superconductivity [2], half metal [3], ferromagnetism [4], magnetoresistance [5], magnetodielectric effect [6], excellent luminescence properties [7], etc., depending on the magnetic and electric characteristics of B and B′. More recently, a burst of research activities on dielectric properties of double perovskites has been triggered by the discovery of the magnetodielectric effect in La_2NiMnO_6 [6]. Several stunning dielectric properties were reported in a number of double perovskites. In spite of the magnetodielectric effect found in La_2NiMnO_6 [6–8] and La_2CoMnO_6 [9], colossal dielectric constants (dielectric constant larger than 10^3) also have been reported [10–12]. The results reported by Castro et al. revealed that Ba_2BiSbO_6 show multi-relaxations [13]. Lin et al. reported a relaxor-like dielectric behavior in La_2NiMnO_6 [14] and La_2CoMnO_6 [15]. In addition, double perovskites have been widely reported to be promising dielectric materials for microwave applications due to their adequate dielectric responses at high frequencies [16–19].

A new double-perovskite Ca_2CoNbO_6 (CCNO) had been synthesized recently via solid-state reaction technique by Shaheen et al. [20]. CCNO was reported to have a monoclinic symmetry with space group $P2_1/n$ and almost identical ionic radii of cation leading to anti-site disordering of 31% [20]. It was felt that CCNO could be yet another promising dielectric material. The details concerning the low-temperature dielectric response of CCNO as functions of frequency and temperature were reported in this article.

2 Experimental details

Polycrystalline samples of CCNO were prepared by the conventional solid-state reaction method. Stoichiometric

G. J. Wang · C. C. Wang (✉) · S. G. Huang · X. H. Sun · C. M. Lei · T. Li · J. Y. Mei
Laboratory of Dielectric Functional Materials, School of Physics & Material Science, Anhui University,
Hefei 230039, China
e-mail: ccwang@ahu.edu.cn

amounts of high-purity (99.99%) $CaCO_3$, Co_3O_4, and Nb_2O_5 were thoroughly mixed by ball milling for 15 h. The mixture was first heated at 1,173 K with a heating rate of 3 K/min for 24 h followed by furnace cooling. Then the mixture was reground, pressed into pellets with the size of 12 mm diameter and about 1 mm thickness, and sintered at 1,523 K with a heating rate of 3 K/min in air for 20 h followed by furnace cooling. The crystal structure was characterized by X-ray diffraction (XRD) using a Beijing Purkinje General Instrument XD-3 diffractometry with Cu Kα radiation. The morphology and microstructure of the sintered samples were characterized by a field emission scanning electron microscopy (SEM) (Model S-4800, Hitachi Co., Tokyo, Japan). The temperature-dependent dielectric properties were obtained using a Wayne Kerr 6500B precise impedance analyzer with the sample mounted in a holder placed inside a PST-2000HL dielectric measuring system. The system with liquid nitrogen can provide a temperature range from 100 to 333 K. The temperature variations were automatically controlled by a Stanford temperature controller with a heating rate of 2 K/min. The amplitude of the ac measuring signal was 100 mV rms. Annealing treatments were performed in flowing (200 ml/min) O_2 and N_2 (both with purity >99.999%). Before measuring, electrodes were made by printing silver paste on both sides of the disk-type samples and then fired at 873 K for 1 h in order to remove the polymeric component.

3 Results and discussion

XRD pattern shown in Fig. 1 indicates that the as-sintered disks are of single phase with monoclinically distorted perovskite-related structure. The calculated lattice parameters of a=0.54944(1) nm, b=0.57020(8) nm, c=0.79036(4) nm, β=89.87(7)° are fairly consistent with those reported (a=0.54797(1) nm, b=0.56051(1) nm, c=0.78119(2) nm, β=89.96(1)°) by Shaheen [20]. A typical SEM micrograph of CCNO is shown in the inset of Fig. 1. A uniform grain formation is observed. From the micrograph it can be seen that the microstructure is inhomogeneous. The grain size of CCNO is in the range of 0.5–7 μm.

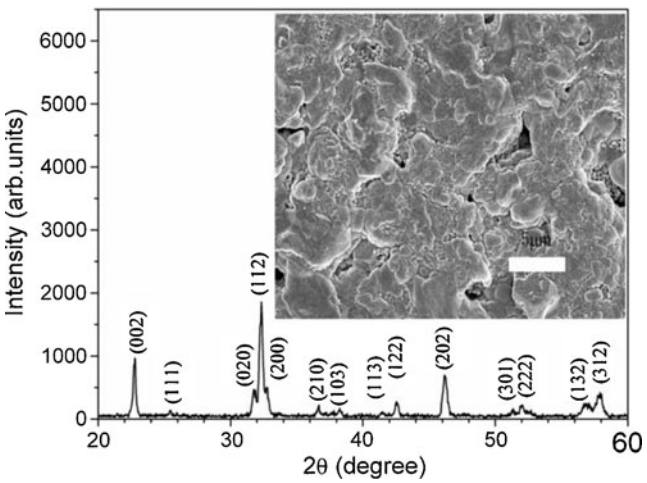

Fig. 1 XRD pattern of CCNO polycrystalline powders. The inset shows the SEM image of the as-sintered surface for a CCNO pellet

The temperature dependences of the dielectric constant (ε'), dielectric loss tangent (tan $\delta = \varepsilon''/\varepsilon'$), and dielectric loss ($\varepsilon''$) under several frequencies of the CCNO pellet with thickness of 0.92 mm were shown in Fig. 2(a), (b), and (c), respectively. It is seen that the $\varepsilon'(T)$ exhibits a steplike decrease as the temperature, T, decreases from room temperature to about 173 K. The steplike decrease shifts to higher temperatures with increasing measuring frequencies accompanied by a small hump in corresponding tan δ (in the range of ~200–300 K). The hump can be clearly identified

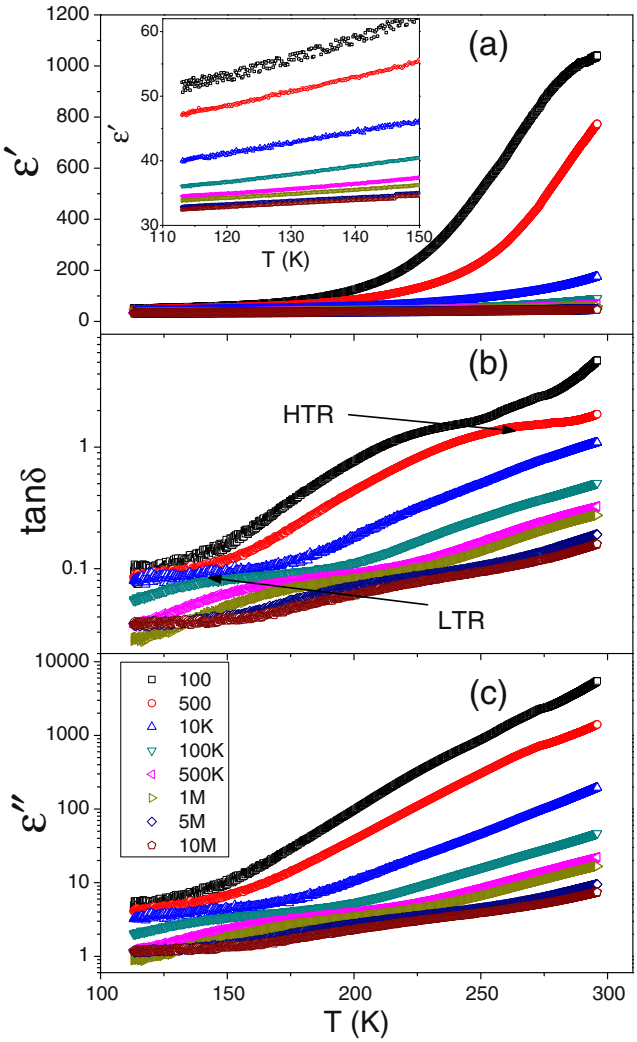

Fig. 2 Temperature dependence of the dielectric constant (**a**), loss tangent (**c**), and imaginary (**c**) part of the complex permittivity for a thick CCNO pellet measured at different frequencies. The inset is an enlarged view of the dielectric constant in the low temperature range

in the curves of tan δ and obtained at 100 and 500 Hz. For curves measured at frequency higher than 500 Hz, the hump moves out of the measuring temperature window. This behavior indicates that there exists a thermally activated relaxation in this temperature range. It's a common feature that both $\varepsilon'(T)$ and $\varepsilon''(T)$ for materials exhibiting colossal (giant) dielectric constants, are almost independent of frequency and temperature [21–23], i.e., the two parameters become constants at low enough temperature. Although the curves of $\varepsilon'(T)$measured with different frequencies for the present sample have the tendency to merge into one master curve, they still show notable variations with temperature and frequency down to the lowest measuring temperature of 100 K (shown in the inset of Fig. 2(a)). This implies that a dipolar or an interfacial polarization is still in action. We truly found another set of hump in the curves of tan δ and $\varepsilon''(T)$ at the lowest temperatures. The hump position shifts to higher temperature as the measuring frequency increases. This indicates that there exist two sets of thermally activated relaxations in CCNO ceramic sample. For brevity, the low- and high-temperature relaxations were labeled, respectively, as LTR and HTR as indicated by straight lines in Fig. 2(b). Since both relaxations register as humps, this prohibits us from deducing their positions accurately, and their relaxation parameters cannot be available at the present measurement. To better understand the mechanisms of the two dielectric relaxations in CCNO, it needs other methods to characterize the features of the relaxations.

Two sets of relaxations were frequently reported in different type of materials including double peroskite, and were always ascribed to the contributions from grain and grain boundary [13–20, 24]. The impedance spectrum is extremely advantageous for distinguishing grain and grain boundary contributions [25]. This technique is frequently used to explore and study the dielectric mechanisms of materials with colossal dielectric constants [12, 26–28]. We thus perform impedance analysis on CCNO sample in the frequency range from 100 Hz to 10 MHz. Figure 3 shows the Nyquist plot obtained by plotting Z'' versus Z' (where Z' and Z'' are the real and imaginary parts of the complex impedance Z*) at the temperature of 230, 250, 270, and 290 K. These temperatures were chosen, because the dielectric response is largely contributed from the HTR, but the LTR is still active at high frequencies (please see Fig. 2(b) and (c)). In this case, the impedance spectra should show a main semicircular arc at low frequencies and a weak or even unclear arc at high frequencies. Generally, when two dielectric relaxations are involved, the Nyquist plot usually exhibits two semicircular arcs with the low- and high-frequency ones corresponding to the grain and grain boundary contributions, respectively. As expected, we truly see one major semicircular arc in the Nyquist plot. The arc gradually develops to an asymmetric semicircular as the temperature decreases, indicating the LTR becomes more and more active. The impedance data can be best modeled by

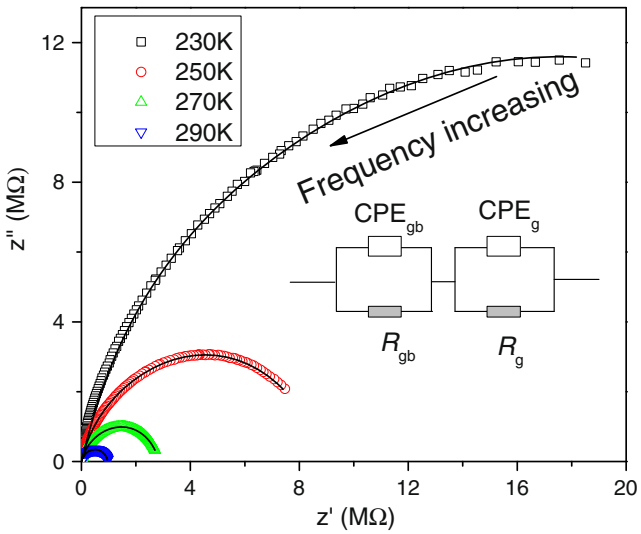

Fig. 3 Nyquist plot of the impedance of the thick CCNO sample at several temperatures. The inset displays the equivalent fitting circuit. The fitting results were shown as *solid curves* in the inset

invoking an equivalent circuit consisting of two serially connected *R*-CPE units, one for the grain and the other for the grain boundary, each containing a resistor (*R*) and a constant phase element (CPE) (instead of ideal capacitor) in parallel as depicted in the inset of Fig. 3. The impedance of the element is defined by [29]

$$1/Z_{CPE} = Q(j\omega)^n \tag{1}$$

where $\omega(=2\pi f)$is the angular frequency, j is the square root of -1, Q and $n(0\leq n\leq 1)$ are adjustable parameters independent of the temperature. The fitted impedance curves shown as solid lines in Fig. 3 agree perfectly with the experimental data. The resultant parameters were listed in Table 1, from which we can see that both the grain and grain boundary resistances obey the Arrhenius relation

$$R = R_0 \exp(E_a/k_B T) \tag{2}$$

where R_0 is the pre-exponential term, E_a is the activation energy, and k_B is the Boltzmann constant. The linear fits based on Eq. 2 shown as straight lines in Fig. 4 yield the values of E_a=0.16, and 0.40 eV for the grain and grain boundary, respectively. The E_a value of the grain boundary is found to be closely related to the activation energy of defect dipolar relaxation caused by oxygen and cobalt vacancies reported in $CoTiO_3$ (0.35 eV) [30]. In CCNO, oxygen vacancies are the intrinsic defects as Rietveld refinement of oxygen occupancies indicates that CCNO is slightly oxygen deficient [20]. On the other hand, the cobalt as a volatile element is easy to be lost during the sintering process as reported by many authors [30, 31]. Therefore, both the negatively and positively charged vacancies coexist in the sample, which may connect with each

Table 1 Fitting parameters of Fig. 3 based on the equivalent circuit

Temp. (K)	Grain			Grain boundary		
	R_g (MΩ)	Q_g (Ω^{-1} m^{-2} S^{-n})	n_g	R_{gb} (MΩ)	Q_{gb} (Ω^{-1} m^{-2} S^{-n})	n_{gb}
230	2.82	7.37×10^{-10}	0.98	31.50	8.95×10^{-10}	0.78
250	1.19	1.31×10^{-9}	0.87	7.73	1.2×10^{-9}	0.80
270	0.83	1.73×10^{-9}	0.81	2.01	1.76×10^{-9}	0.83
290	0.50	1.87×10^{-9}	0.80	0.47	2.92×10^{-9}	0.86

other to form defect dipoles and make contributions to both electric and dielectric excitations. In this case, the dielectric properties of CCNO are expected to be easily tuned by annealing in oxidative and reduced atmospheres. This point is confirmed by dielectric measurements in another thinner sample with thickness of 0.66 mm.

Figure 5 displays the dielectric properties of the thinner CCNO pellet before (as-prepared) and after several post-annealing processes at a number of frequencies. The annealing processes consist of several consecutive steps: firstly, the pellet was annealed in O_2 at 1,073 K for 2 h, denoted as A1; then, annealed in N_2 at 1,073 K for 2 h after A1, denoted as A2; and finally, annealed again in O_2 at 1,073 K for 2 h after A2, denoted as A3. After each step, dielectric properties were measured as a function of temperature. Compared with the thicker sample, two notable features for the as-prepared thinner sample can be seen: (1) the values of $\varepsilon'(T)$greatly decreased and (2) the thinner sample shows two distinct relaxations (with the LTR appears between 100 and 250 K and the HTR occurs between 250 and 340 K), each characterized by a frequency-dispersed increase in $\varepsilon'(T)$accompanied by a peak in the corresponding curve of loss tangent. The first feature might be because that the concentration of the oxygen vacancy is very sensitive to the sample preparation process and sample geometry as reported in $CaCu_3Ti_4O_{12}$ [32]. The reduction of sample thickness leads to the great decrease in the number of defect dipole, since the Co deficient easily occurs at the out most part of the sample as reported in other volatile element, like Ag in $CaCu_3Ti_4O_{12}$ [33]. The ionization of

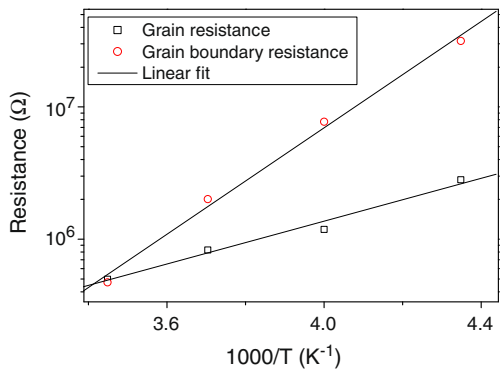

Fig. 4 Arrhenius plots of the resultant grain and grain boundary resistances. The *straight lines* are the linear fitting results

oxygen vacancies creates negatively charged electrons, while the cobalt vacancies produce positively charged holes. The conductivity of the sample depends on the competitive process between electrons and holes. After recombination, only the remaining net carriers have contribution to the conductivity. This fact gives rise to an unremarkable background, and as a consequence, the relaxations become more pronounced which lets us evaluate the relaxation parameters of the relaxations. The frequency dependence of peak temperature is plotted in Fig. 6 based on the Arrhenius relation:

$$f = f_0 \exp(-E_a/k_B T_m) \tag{3}$$

where f is the measuring frequency, f_0 is the pre-exponential factor, and T_m is the temperature where the maximum loss tangent occurs. Linear fits yield the values of f_0 and E_a to be 5.78×10^9 Hz, 0.37 eV for the HTR, and 2.63×10^{10} Hz, 0.13 eV for the LTR. The values of activation energy are almost the same as those deduced from the impedance spectra, indicating that the resistance and dielectric relaxation are closely related.

After process A1, a notable decrease in dielectric constants was observed as compared with the as-prepared state. This is because the oxygen vacancies were largely annihilated by the O_2-annealing process. In other words, this means an increase in the number of the remaining holes that causes a nearly exponentially increasing background of the loss tangent as clearly seen from the Fig. 5. Consequently, the HTR can only be identified by very weak humps as indicated by the arrow. Additional, HTR shifts to lower temperature by about 55 K after O_2-annealing treatment. This feature agrees quite well with that reported in $CoTiO_3$ [30] confirming that the HTR is related to the defect dipolar relaxation. However, the O_2-annealing treatment has no observed influence on the LTR, indicating that the relaxing species are positively charged carriers. Although oxygen vacancies carry positive charge, we can immediately rule out the possibility that the relaxing species are related to oxygen vacancies because of the low activation energy (0.13 eV) [34]. Therefore, these carriers can be identified as holes. Hole jumping between spatially fluctuating lattice potentials give rise to dipolar effect [35]. As temperature decreases, the involved charge carriers become sufficiently localized. In other words, their inertial mass (the eigenfrequency) becomes sufficiently large (low). Then, they cannot

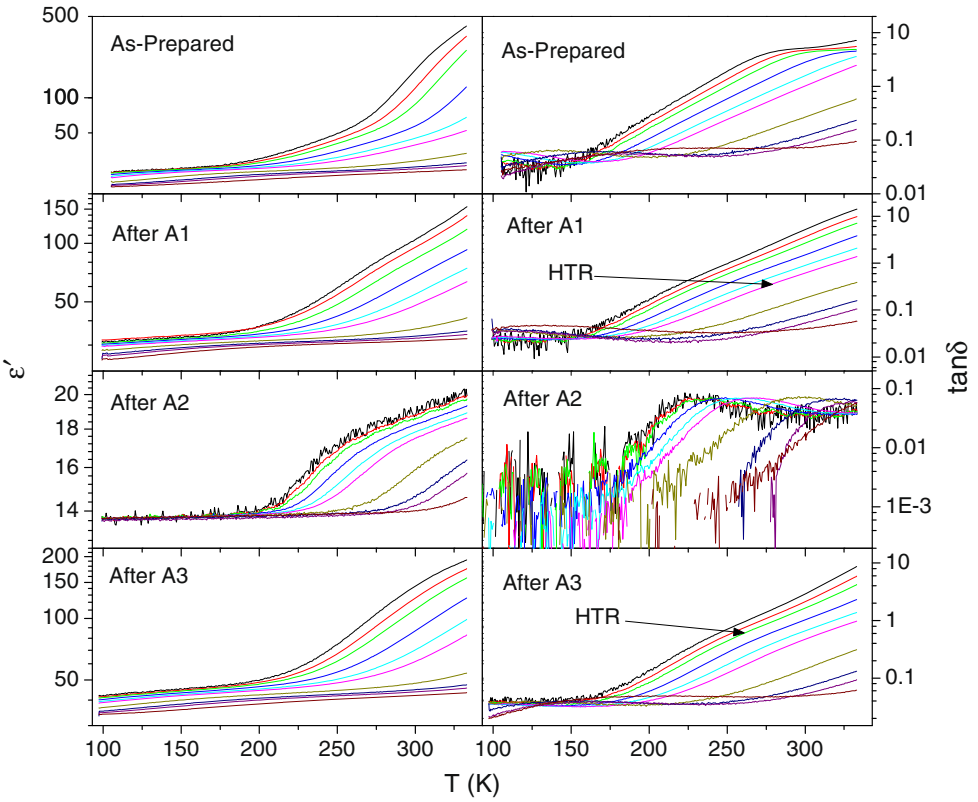

Fig. 5 Temperature dependence of ε' and tan δ for a thin CCNO pellet before (as-prepared) and after several annealing processes at the measuring frequencies of 300, 500, 800, 2 k, 5 k, 10 k, 100 k,500 k, 1 M, and 5 MHz (from top to bottom)

follow the field variations and the resulting effect is a dielectric relaxation with the relaxation peak appearing at the temperature where the eigenfrequency of the carriers equals the frequency of the applied field.

After process A2, two pronounced features can be summarized: (1) the LTR disappears completely, and (2) the values of $\varepsilon'(T)$decreases about one order of magnitude, while tan δ decreases about two orders of magnitude. Since there is no increasing background in the loss tangent indicating that the number of oxygen vacancies was raised by N_2-annealing process to almost the same level as that of cobalt vacancies. The

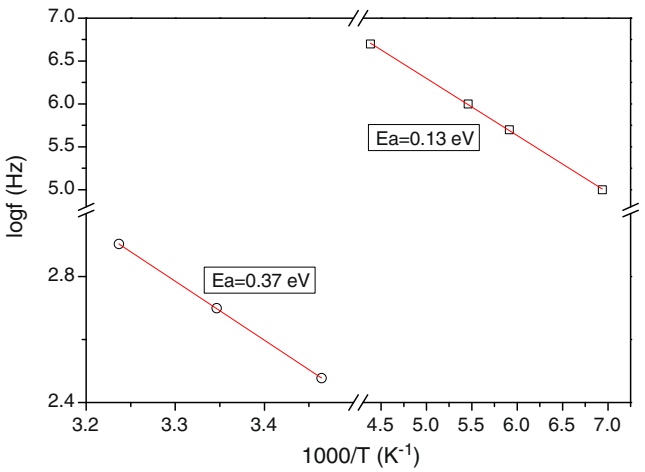

Fig. 6 Arrhenius plots of the low- and high-temperature relaxations obtained from the as-prepared thin pellet

holes are expected to be completely recombined by the electrons. So, there are no net carriers that can make contribution to conductivity. The observed dielectric loss is purely due to the dielectric relaxation and thus shows very small values. Meanwhile, the LTR disappears as the disappearance of the relaxing species that leads to the great decreases in $\varepsilon'(T)$. This result substantially confirms the inference that the LTR is related to the hole.

After process A3, the dielectric properties, as expected, recover to the state before A2. This implies that the number of the cobalt vacancies overwhelms that of the oxygen vacancies. So, the LTR dominated by hole appears again, and the nearly exponential increasing background of the loss tangent regains due to notable conductive contribution from the hopping holes, which in turn, causes the HTR that can be seen by the small humps as indicated by the arrow in Fig. 5. These results demonstrate that the LTR and HTR are associated with the dipolar effect caused the hopping holes and the connection of oxygen and cobalt vacancies, respectively.

4 Conclusions

In summary, we have performed systematically investigation on dielectric properties of double-perovskite CCNO ceramics. We find that: (1) both oxygen and cobalt vacancies coexist in the sample. (2) The electric and dielectric properties are closely linked. The dielectric properties of

CCNO are dominated by the competitive contribution of the two kinds of defects and hence can be tuned by post-annealing in different atmospheres. (3) Two Debye-like dielectric relaxations were observed with activation energy around 0.13 eV and 0.37 eV for the low- and high-temperature relaxations, respectively. The low-temperature relaxation was argued to be related to dipolar effect created by hopping holes, while the high-temperature relaxation was suggested to originate from the defect polarization due to the connection of oxygen and cobalt vacancies.

Acknowledgments The authors thank financial support from National Natural Science Foundation of China (Grant No 11074001).

References

1. R.M. Hazen, Sci. Am. **258**, 54 (1988)
2. A.W. Sleight, J.L. Gillson, P.E. Bierstedt, Solid State Comm. **17**, 27 (1975)
3. J.B. Philipp, P. Majewski, L. Alff, A. Erb, R. Gross, T. Graf, M.S. Brandt, J. Simon, T. Walther, W. Mader, D. Topwal, D.D. Sarma, Phys. Rev. B **68**, 144431 (2003)
4. See, for example, N. Rama, J. B. Philipp, M. Opel, V. Sankaranarayanan, R. Gross, and M.S. Ramachandra Rao, J. Phys. D: Appl. Phys. **40**, 1430 (2007), and references cited there.
5. K.-I. Kobayashi, T. Kimura, H. Sawada, K. Terekura, Y. Tokura, Nat. (Lonedon) **395**, 677 (1998)
6. N.S. Rogada, J. Li, A.W. Sleight, M.A. Subramanian, Adv. Mater. **17**, 2225 (2005)
7. P.A. Tanner, Z. Pan, Inorg. Chem. **48**, 11142 (2009)
8. P. Padhan, H.Z. Guo, P. LeClair, A. Gipta, Appl. Phys. Lett. **92**, 022909 (2008)
9. M.P. Singh, K.D. Truong, P. Fournier, Appl. Phys. Lett. **91**, 042504 (2007)
10. Y.Q. Lin, X.M. Chen, Appl. Phys. Lett. **96**, 142902 (2010)
11. W.Z. Yang, M.M. Mao, X.Q. Liu, X.M. Chen, J. Appl. Phys. **107**, 124102 (2010)
12. K.R.S. Preethi Meher, K.B.R. Varma, J. Appl. Phys. **105**, 034113 (2009)
13. M.C. Castro, C.W.A. Paschoal, F.C. Snyder, M.W. Lufaso, J. Appl. Phys. **104**, 104114 (2008)
14. Y.Q. Lin, X.M. Chen, X.Q. Liu, Solid State Comm. **149**, 784 (2009)
15. Y.Q. Lin, X.M. Chen, J. Am. Ceram. Soc. **94**, 782 (2011)
16. A.N. Salak, O. Prokhnenko, V.M. Ferreira, J. Phys. Condens. Matter **20**, 085210 (2008)
17. J.J. Bian, K. Yan, Y.F. Dong, Mater. Sci. Eng. B **147**, 27 (2008)
18. L.A. Khalam, S. Thomas, M.T. Sebastian, J. Am. Ceram. Soc. **90**, 2476 (2007)
19. F. Zhao, Z.X. Yue, Z.L. Gui, L.T. Li, Jpn. J. Appl. Phys. **24**, 8066 (2005)
20. R. Shaheen, J. Bashir, Solid State Sci. **12**, 1496 (2010)
21. M.A. Subramanian, D. Li, N. Duan, B.A. Reisner, A.W. Sleight, J. Solid State Chem. **151**, 323 (2000)
22. A.P. Ramirez, M.A. Subramanian, M. Gradel, G. Blumberg, D. Li, T. Vogt, S.M. Shapiro, Solid State Comm. **115**, 217 (2000)
23. C.C. Homes, T. Vogt, S.M. Shapiro, S. Wakimoto, A.P. Ramirez, Sci. **293**, 673 (2001)
24. C.C. Wang, Y.M. Cui, L.W. Zhang, Appl. Phys. Lett. **90**, 012904 (2007)
25. R. Gerhardt, J. Phys. Chem. Solids **55**, 1491 (1994)
26. W. Li, R.W. Schwartz, Phys. Rev. B **75**, 012104 (2007)
27. G.H. Cao, L.X. Feng, C. Wang, J. Phys. D Appl. Phys. **40**, 2899 (2007)
28. M. Li, D.F. Zhang, W.Y. Wang, G. Wang, X.L. Chen, J. Phys. D Appl. Phys. **43**, 295405 (2010)
29. D. Morrison, D.J. Jung, J.F. Scott, J. Appl. Phys. **101**, 094112 (2007)
30. C.C. Wang, L.W. Zhang, J. Phys. D Appl. Phys. **40**, 6834 (2007)
31. T. Ogawa, M. Ono, M. Fujiwara, Jpn. J. Appl. Phys. **34**, 5306 (1995)
32. B.A. Bender, M.J. Pan, Mater. Sci. Eng. B-Solid State Mater. Adv. Technol. **117**, 339 (2005)
33. C.C. Wang, Y.J. Yang, L.W. Zhang, M.Y. Cui, G.L. Xie, B.S. Cao, Scripta Mater. **54**, 1501 (2006)
34. G.M. Keith, K. Sarma, N.M. Alford, D.C. Sinclair, J. Electroceram. **13**, 305 (2004)
35. A.K. Jonscher, Nat. (London) **253**, 717 (1975)